Available online at www.ijapie.org

International Journal of Advanced
Production and Industrial Engineering

IJAPIE-SI-MM 510 (2017) 63–70

Special Issue on

MATERIALS
&
MANUFACTURING

Review Method for Regasification and Dissociation Rate of Methane Hydrate

S. R. Kumbhar*, O. B. Surve
(Rajarambapu Institute of Technology, Sangli, Maharashtra- 416414, India)
**Email: sanjay.kumbhar@ritindia.edu*

Abstract : First case dry water (DW) is recently demonstrated to be an effective medium for methane storage in hydrate form. To measurement their formation and dissociation rates and storage capacity. Storage capacity of MH increases at least 10% by using DW relative to using Sodium dodecyl sulphate solution also control on pressure temperature (P-T) curve condition on the induction and reaction time of DW-MH formation. In second case effect of methane hydrate dissociation at different temperature using triaxial compression test on methane hydrate-bearing sediment after hydrate dissociation time of 0h, 1h, 6h, 12h or 24h the mechanical properties of sediment during hydrate dissociation at different temperatures. When increase in the MH dissociation time the failure strength and initial yield strength both decreased, and the rate of decline failure strength was faster at higher temperature.

Keywords: Dry water, Methane gas hydrate, Hydrate dissociation, Methane hydrate-bearing sediments stability.

I. INTRODUCTION

Gas hydrates, also known as clathrates, are ice-like, crystalline inclusion compounds composed of water molecules surrounding gas molecules (usually methane) under certain pressure and temperature [1]. As one volume of methane hydrate (MH) can yield as much as 180 v/v stp methane [2], it is suggested that it may be economically feasible to transport natural gas in a hydrated form. In particular, the transportation cost is expected to be 18–24% lower than with liquefied natural gas (LNG) transportation [3,4], and the transportation is more secure than LNG or pipeline transportation [5].

The methane hydrate storage chain consists of three main parts, the hydrate formation, transportation and regasification [6]. Several works have been done to promote the application industry [7]. For example, it is found that the hydrate formation conditions may change to be much milder with various additives [8–10], while the formation rate and storage capacity can be largely enhanced by stirring, bubbling, or adding surfactants [11–15]. Recently, a more attractive method, using dry water as a medium for MH formation, has been used to promote the MH formation rate and storage capacity significantly [16,17].

DW is a free-flowing powder prepared by mixing water and hydrophobic silica particles (H18) at high speeds [18]. The highly distributed gas-liquid interface in “dry water” powder can be used to greatly increase the rate of heterogeneous gas-liquid reactions [19]. Wang et al. [16] is probably the first one who report methane storage in DW–MH. Using DW in storing system, they have dramatically enhanced the formation rate and methane uptake of MH. In their work, the methane uptake kinetics in DW–MH at 0°c were investigated and shown that the CH4 capacity is related to the mixing speed of making DW.

Hydrate-bearing sediments during hydrate dissociation have been studied further. Lu et al. (2008) studied the mechanical properties of a tetrahydrofuran hydrate deposit and found that the mechanical properties were affected by hydrate dissociation. Masui et al. (2007) studied the compaction behavior of methane hydrate- bearing sediments during hydrate dissociation. Lee et al. (2010) studied the volume change rules for tetrahydrofuran hydrate- bearing sediments during hydrate dissociation. Hyodo et al.(2013, 2014) studied the deformation behavior of isotropically and K0 consolidated methane hydrate-bearings and which dissociated by heating and depressurizing.

Although there has been much research, as mentioned above, on the mechanical properties of hydrates or hydrate-bearings- sediments, there has been little investigation of the mechanical properties of methane hydrate-bearing sediments during the de- composition process of hydrate under thermal stimulation. In this review, to study the effect of methane hydrate dissociation at different temperatures on the stability of methane hydrate-bearing sediments, these porous sediments were made in the laboratory, and a series of triaxial compression tests of the sediments with 40% porosity were performed during hydrate dissociation at different temperatures. According to the literature (Fu etal.2010), part of gas hydrates were uniformly distributed in dispersed state in pore space. Thus, in this review, focus on the homogeneous methane hydrate-bearing sediments.

II. CASE STUDY 1

Dry water preparation

The hydrophobic silica nanoparticles (H18) were kindly supplied by Wacker Chemie. In a high-speed mixing blender (Blendtec, Glass Jug Blender, Part #40-501, 1000 milliliter), 5 g H18 was added to 95g de-ionized water. Mixing was carried out at three different speeds (speed 1:12,000 rpm; speed 2:17,000 rpm; speed 3:22,000 rpm) for 90 s. The DW was produced as a free-flowing white powder which could be poured from one vessel into another (Fig. 1).

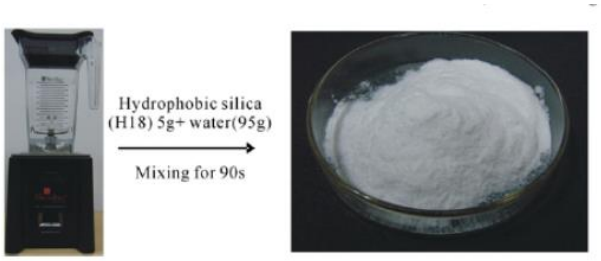

Fig.1. Dry water prepared with 5 g hydrophobic silica nanoparticles (H18) and 95 g water mixing at 22,000 rpm for 90 s.

Hydrate formation

The apparatus for hydrate formation is shown in Fig. 2. It is composed of four functioning units: (1) a high-pressure reaction cell (max volume 130 cm3) for simulating appropriate pressure and temperature of hydrate formation, in which there is a platinum (Pt100) resistance thermometer with precision of ±0.1 °C used for measuring the temperature of the sample, (2) a gas compressor and a pressure transducer (Shanghai Tianmu company, precision ±0.1 MPa) responsible for gas pressure control, (3) a cooling system and jacketed coolant around the reaction cell for temperature control, and (4) a computer system for measuring and interval-logging data of temperature, pressure and time. An easy-unlock switch was mounted on the reaction cell so that the hydrate samples can be rapidly taken out after it is formed. For more details of the apparatus, see reference.

In each experiment, 20 g of DW was loaded into the reaction cell for MH formation. Two types of controls on P–T condition were conducted to form hydrate. In type I, high pressure methane gas (8–9MPa) was introduced into the vessel before temperature decreasing. In type II, Gas was introduced after the temperature is at a certain temperature (~3 °C) which is directly conducive for hydrate formation. In this way, the induction and reaction time of the hydrate formation under different control conditions were investigated (reaction time means the interval time between time point of hydrate begins to form to the time point of hydrate formation finishes). After the DW–MH was formed, high pressure gas was released and the easy-unlock switch was rotated a few circles to open the reaction cell within 1–2 min. And then the DW–MH was taken out, and submerged into liquid nitrogen for following measurements.

Induction and reaction time of DW-MH formation

The formation conditions of DW and DW–MH samples are shown in Table, and the hydrate formation processes by two different types of P-T condition-controls are shown in Fig. 3. As shown in the formation process of DW–MH-1 (Fig. 3, left), the induction time, which means the interval time between time point of P-T conditions become conducive for methane hydrate formation to the time point of hydrate begins to form, was about 243 min. And the reaction time of hydrate formation of DW–MH-1 was about 166 min. The induction and reaction time were much shorter with the second type of P-T condition-control, however. As shown in Fig. 3, right, the induction time and reaction time of sample DW–MH-2 were about 4 min and 70 min, respectively, when hydrate was formed under a certain temperature (~3 °C) which is directly conducive for hydrate formation.

Our results are similar to Wang et al. [16], who have investigated the first type of P-T condition for DW–MH formation (although their DW is prepared at a different mixing speed of 19,000 rpm). In their studies, the reaction time of DW–MH was about 160 min (when gas capacity achieve about 158 v/v STP), which is very close to the first type result of 166 min in our experiments. Notably, the reaction time under the second type of P–T condition is much shorter than that under the first type. So we formed two other samples, DW–MH-2 and DW–MH-3, under the second type of P–T condition to investigate the effect of mixing speed of making DW on the induction time and reaction time (Table and Fig. 4). The results indicate that when the mixing speed is lower, the induction time will be a little longer while the reaction time is remained as 70–77 min. Thus, from the above experiments, it is suggested that DW–MH may be formed under the second type of P–T condition to enhance the friction rate.

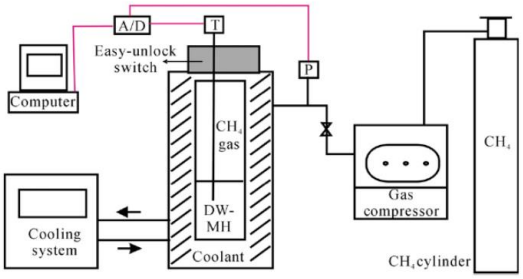

Fig. 2. Schematic diagram of the hydrate-formation apparatus

Table 1
Parameter of DW-MH samples

Sample No.	Mixing speed of DW	P-T condition	Induction time (min)	Reduction time (min)
DW-MH-1	Speed 3	Type I	243	166
DW-MH-2	Speed 2	Type II	32	75
DW-MH-3	Speed 1	Type II	8	70
DW-MH-4	Speed 3	Type II	4	70
DW-MH-5	Speed 3	Type II	6	77

Note: type I: high pressure gas (8–9 MPa) was introduced into the reaction cell under room temperature, then the temperature was decreased to form hydrates; type II: after the reaction cell was cooled to ~3 °C, high pressure gas (8–9 MPa) was introduced to form hydrates.

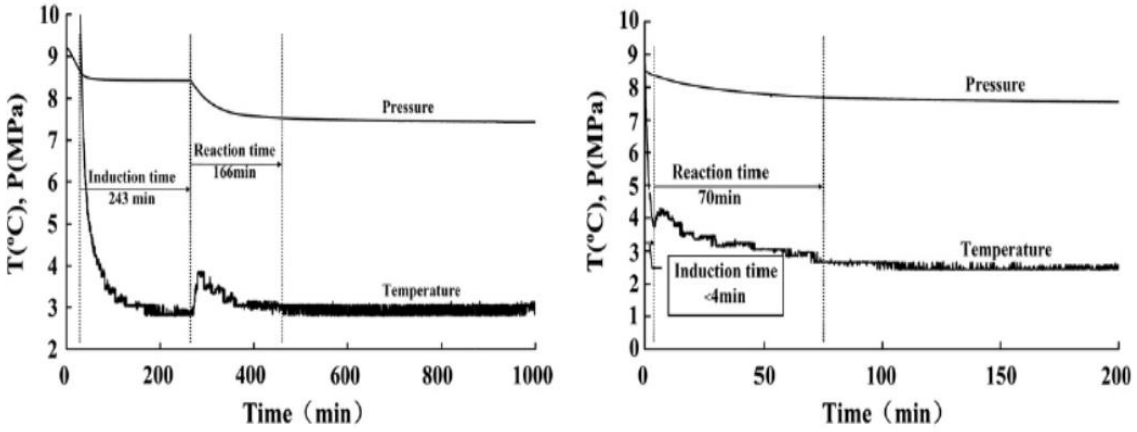

Fig.3. P-T changes during hydrate formation in a scaled system (left, DW-MH-1; right, DW-MH-4)

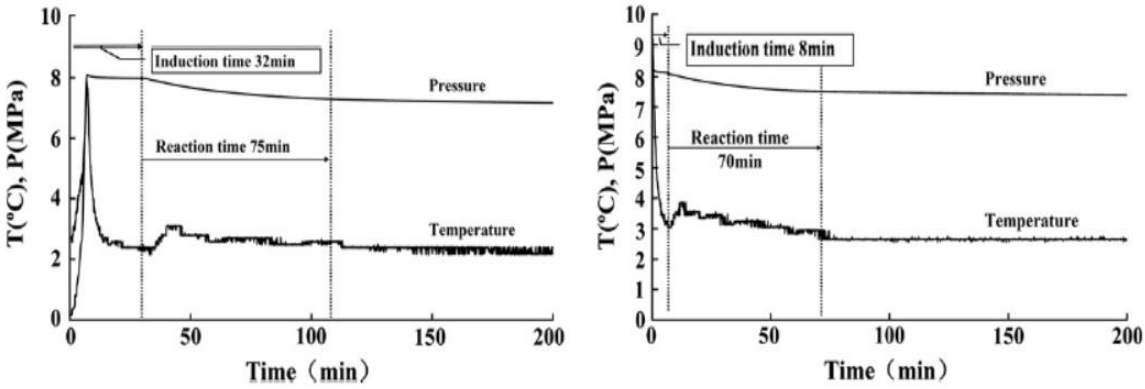

Fig. 4. Induction time and reaction time of DW–MH-2 (left, DW prepared at mixing speed 3) and DW–MH-3 (right, DW prepared at mixing speed 1)

Dissociation rate and self-preservation of DW-MH

A typical dissociation process of DW–MH-1 is shown in Fig. 5. DW–MH sample was placed in sample test tube of the storage capacity measurement apparatus (Fig. 6), and the test tube was partly submerged into liquid nitrogen so that hydrate can be stable. After the whole system was vacuumed, the liquid nitrogen cup was moved away and the DW–MH sample was warmed by room temperature. About 3 min later, the pressure began to increase, which indicates that DW–MH start to dissociate. In Fig. 5, it shows that the whole dissociation process can be described by four stages. At the first stage, the dissociation rate is very rapid. Almost 55% of total methane gas is released in about 2 min. The dissociation rate at the second stage is much lower (~15 times lower) than

that at the first stage, however, probably it is caused by the self preservation behavior of MH [25]. And then the dissociation rate rebounds at the third stage since the methane gas burst after the ice trap is thawed. However, the rate is lower than that at the first stage because the total mass of gas is smaller. In the last stage, the gas pressure has a small increase by the warm temperature. About the self preservation behavior of DW–MH during hydrate dissociation, it occurred in our experiments after that more than half of the methane gas was released. Thus, more efforts need to be made to improve usage of this behavior during the MH storage chain.

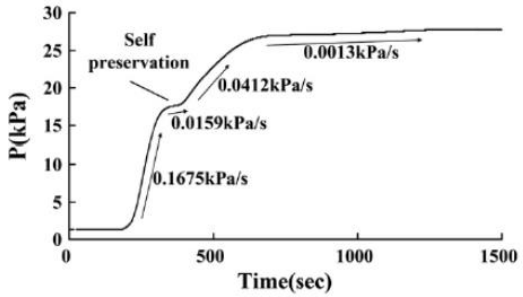

Fig. 5. Dissociation process of sample DW–MH-1 under free space and room temperature (~20 °C).

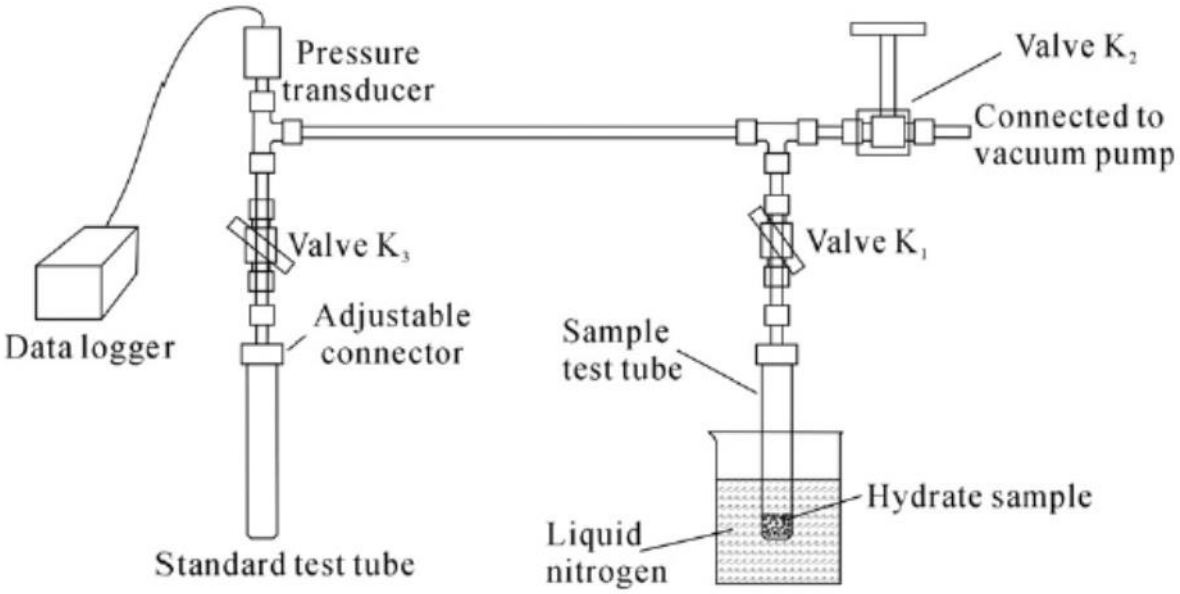

Fig. 6. Schematic diagram of apparatus for measuring storage capacity and dissociation rate of gas hydrates

III. CONCLUSIONS (Case I)

In this paper, the results of direct measurements on formation rate, structural characteristics, storage capacity and dissociation rate of five DW–MH samples were reported. The conclusions are made as follows: (1) the formation rate can be improved by controlling the P-T condition of hydrate formation, i. e. the induction and reaction time of DW–MH formation are 243 min and 166 min respectively when the reaction cell is pressurized before cooled, while they are 4 min and 70 min respectively when the reaction cell is cooled first; although the formation time is reduced compared with Wang et al. [16], further reduction of DW–MH formation time may possibly be made by a more appropriate P–T condition; (2) DW can be used to increase at least 10% of the storage capacity of MH, compared with surfactants such as SDS solutions, further elevation of storage capacity of DW–MH should be focused on enhancing the methane uptake of small cages; and (3) although hydrate dissociation can be prevented by the effect of self preservation, more than half of total methane gas has released before the self preservation occur.

IV. CASE STUDY 2

TESTING APPARATUS AND EXPERIMENTAL PROCEDURE

Ice powder and methane gas were used to generate methane hydrate (Sternetal.,1998). The schematic diagram of the pressure reactor is shown in Fig. 1. Ice powder of an average particle size of 250 mm was manufactured by using an ice crusher to break the prepared freezing distilled water. Then, the ice powder was put into a pressure chamber and methane gas of 99.99% purity was injected in to the reactor through a connecting hose and a constant pressure pump until the pressure of the pressure chamber reached 8 MPa. The reactor was put in to a cold storage freezer at a constant temperature of _10 °C for72h.Then, the methane hydrate was generated and the saturation was in the range of 25–30%.

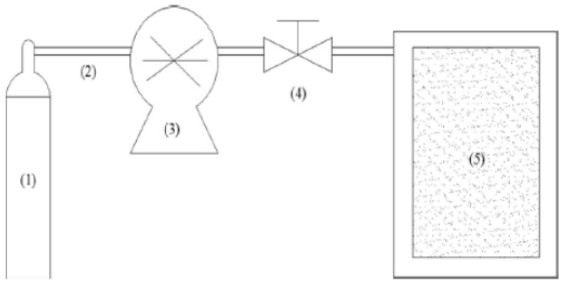

Fig. 1 .The schematic diagram of the pressure reactor for generating methane hydrate.

The prepared methane hydrate ice mixture and kaolin clay were used to manufacture methane hydrate-bearing sediments in the pressure molding device. The grain size distribution curve of kaolin is shown in Fig. 2, and the median particle diameter of kaolin clay is 5.545 μm.

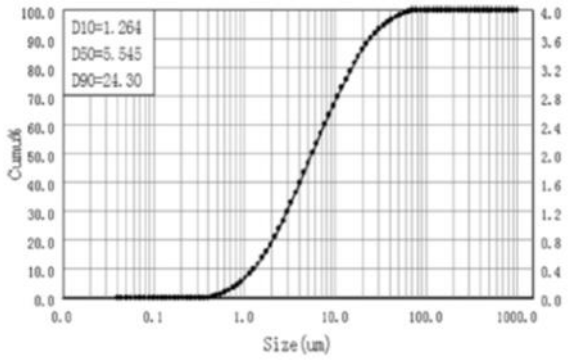

Fig 2. Grain size distribution curve of kaolin clay.

The DDW-600 triaxial testing device is shown in Fig. 4. The prepared samples were removed from the pressure molding device, wrapped with a rubber membrane, and then put into the pressure chamber. After the specimen was jacketed inside the pressure chamber, a predetermined confining pressure and temperature were applied and kept constant during hydrate dissociation. During the shear process, axial stress and axial strain were controlled and measured by a load cell and a displacement sensor.

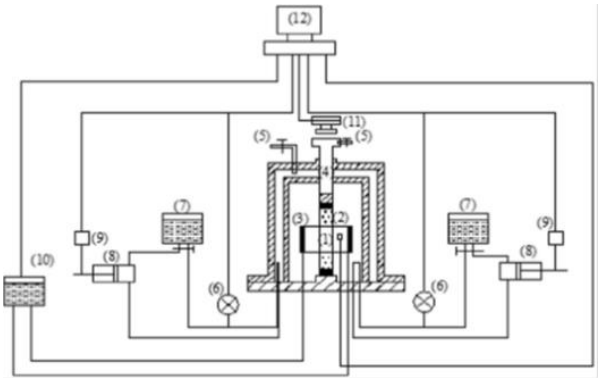

Fig.3. The schematic diagram of the DDW-600 triaxial testing device.(1)Specimen; (2)Thermocouple;(3) Heat exchanger;(4)Axial load cell;(5)Air pressure line; (6)Pressure gauge;(7)Hydraulic oil tank;(8)Plunger pump;(9)High-precision servo motor;(10)Thermostatic bath;(11)Load sensor; and(12)Computer.

Test conditions

The conditions of experimental are shown in table, all of the specimens were consolidated at the confining pressure of 10 MPa for 2h. When the consolidation was finished, the confining pressure and temperature were adjusted to set values (a confining pressure of1 MPa and temperatures of -5 °C, -2 °C, 0 °C, 2 °C and 5 °C). The hydrate dissociated under these conditions according to the phase equilibrium conditions of methane hydrate. The dissociated methane gas entered into the pore space of samples under these conditions without drain. Then, the methane hydrate-bearing sediments after different dissociation times (0h, 1 h, 6h, 12h or 24h) were sheared under undrained conditions and a strain rate of 1%/min.

Table 2
Experimental conditions for the triaxial compression tests on methane hydrate bearing sediments.

Temperature T (°C)	Confining pressure σ_3 (MPa)	Strain rate ε (%/ min)	Dissociation time (h)
-5			0, 6, 24
-2			0, 6, 12, 24
0	1	1	0, 1, 6, 12, 24
2			0, 1, 6, 24
5			0, 1, 6

Stress – strain behaviors

Fig.5 (a)–(e) showed the axial strain-dependence curves of deviator stress after different dissociation time at different temperatures. It can be seen that most of the curves exhibited the shape of a hyperbola, and the stress–strain behaviors indicated that the axial strain fell into two parts: elastic strain and plastic strain. The deviator stress increased nearly linearly with increasing axial strain at the initial loading period, and the deformation mode of the sediments was elastic. With a further increase of axial strain, the stress–strain curves presented a slight hardening behavior, and the slope decreased gradually. At this stage, the specimens had both elastic and plastic deformation. Finally the deviator stress changed relatively little and reached a steady value even if the plastic deformation of the sediments was severe. At this stage, the structure of the specimens was wholly destroyed.

Yu et al. (2011c) observed the stress–strain behaviors of methane hydrate-bearing sediments under subzero temperatures and noted that the temperature had no effect on the strain type. However, Fig. 5 (d) showed a slight strain softening behavior at a temperature of 2°C, and Fig. 5(e) showed that the strain softening behavior appeared at a temperature of 5°C. These results indicated that the strain type was affected by temperatures above freezing and the

deformation mode of methane hydrate-bearing sediments exhibited more obvious strain softening behavior as the temperature increased. According to the literature(Masui etal.,2005; Hyodo et al; 2007; Winters et al; 2007), the cementation between the hydrate particles and soil particles will be destroyed due to the accumulated plastic deformation, which would cause the strain softening behavior. Thus, due to the much greater hydrate dissociation at the temperatures of 2°C and 5°C, the cementation between the hydrate particles and kaolin clay particles was weakened, which resulted in the exhibition of strain softening behavior.

Failure strength

In this study, the deviator stress at15% axial strain was selected as the failure strength of samples. For the specimens with the strain softening behavior, the peak value of deviator stress was taken as the failure strength. Fig.4. Showed the failure strength of the samples versus the dissociation time of the methane hydrates at different temperatures. It can be observed that the hydrate dissociation had a strong effect on the failure strength of methane hydrate-bearing sediments. All of the failure strength values decreased with an increase in the methane hydrate dissociation time at the temperatures of -5 °C, -2 °C, 0 °C, 2 °C and5 °C. During hydrate dissociation, the dissociated methane gas entered into the pore space of specimens which may increase the pore pressure and lead to a decrease of effective confining pressure. Researchers have found that the failure strength of hydrate-bearing sediments decreased with the reduction of effective confining pressure (Hyodo et al; 2013). Consequently, the failure strength of methane hydrate-bearing sediments will decrease during hydrate dissociation.

In addition, at the temperatures above freezing, the rate of the decline of the failure strength during the hydrate dissociation was faster than that at the subzero temperatures. It was found that the failure strength dropped to 0.163 MPa after the hydrate dissociated for 6 h at a temperature of 5 °C and to 0.223MPa after the hydrate dissociated for12 h at a temperature of 2 °C. Compared with the downward trend of failure strength at the subzero temperatures, the failure strength of methane hydrate-bearing sediments decreased more sharply during a short period of dissociation and the sediments almost lost their stability after hydrate dissociation at the above-zero temperatures. However, as shown in Fig. 4, at lower temperatures, the sediments retained a certain amount of strength after dissociation. This phenomenon might be because the original ice within the methane hydrate-ice mixture would melt at temperatures above freezing, dissociated water would not become ice and hydrate dissociated faster at higher temperatures.

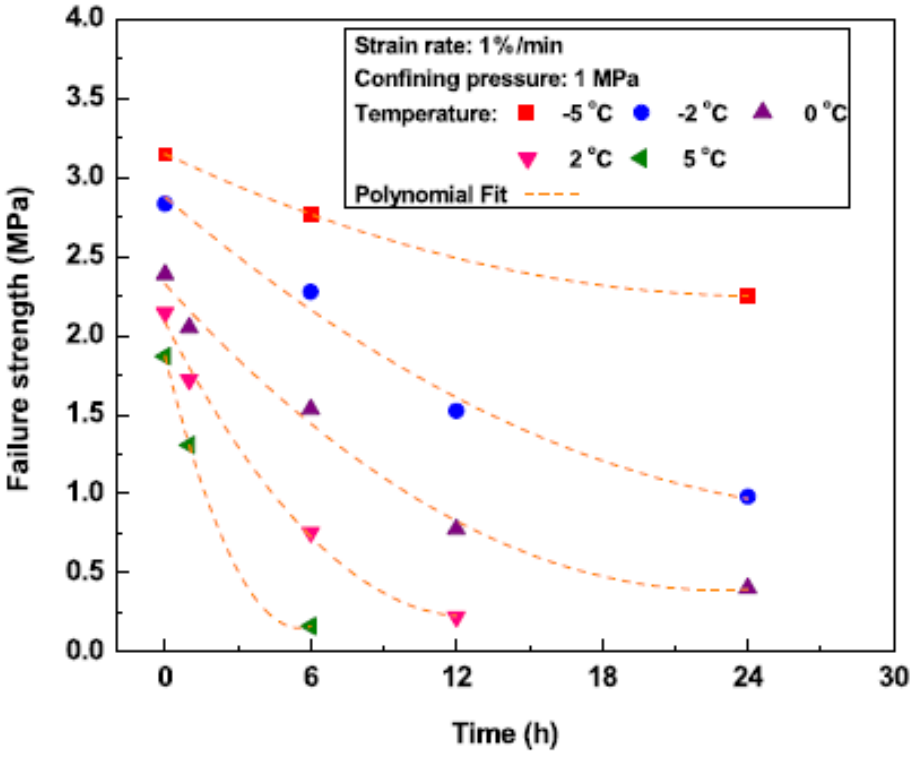

Fig. 4. Effect of hydrate dissociation on the failure strength at different temperatures.

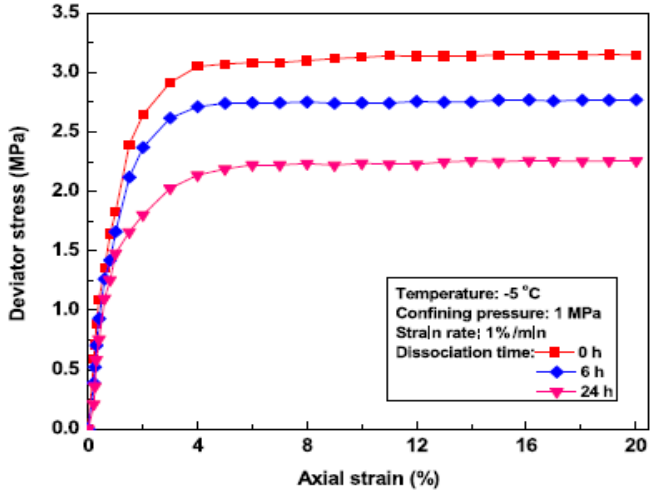

(a) Temperature T= -5 °C

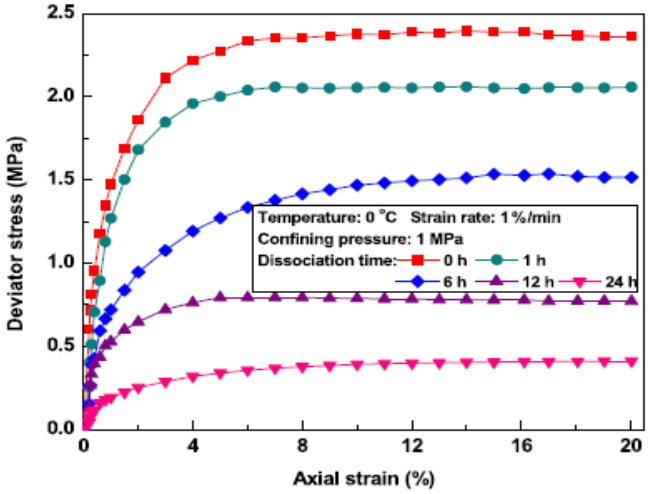

(c) Temperature T= 0 °C

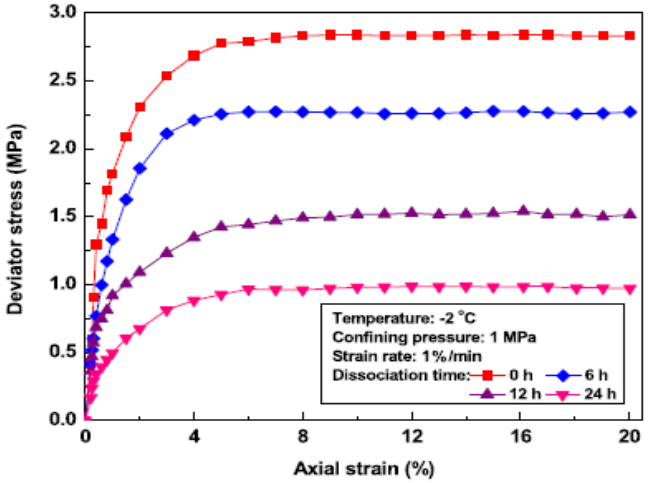

(b) Temperature T= -2 °C

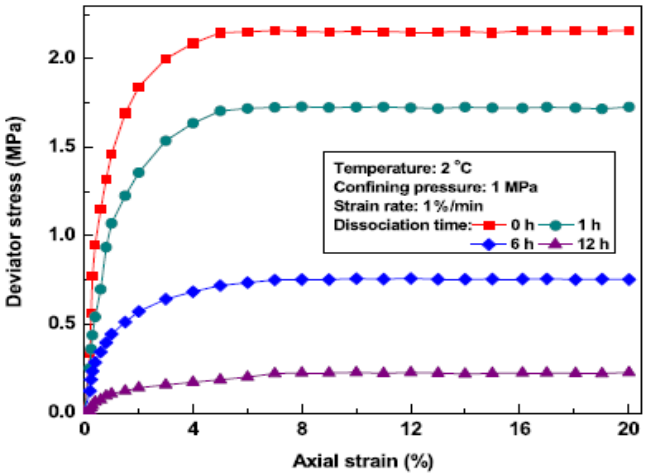

(d) Temperature T= 2 °C

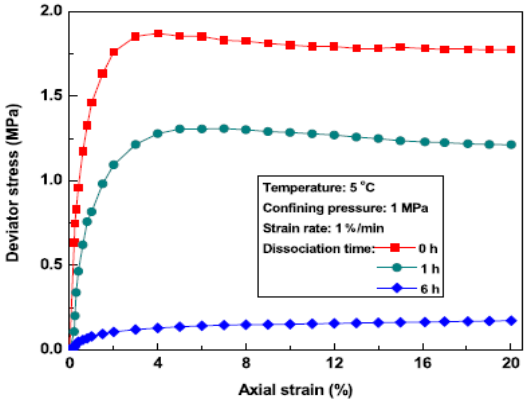

(e) Temperature T= 5 °C

Fig. 5. Stress–strain curves of ϕ 40 artificial methane hydrate-bearing sediments during the hydrate dissociation process at different temperatures. (a)Temperature T= -5 °C. (b)Temperature T= -2 °C. (c)Temperature T= 0 °C. (d)Temperature T = 2 °C. (e)Temperature T= 5 °C.

V. CONCLUSIONS (Case II)

The triaxial compression tests of methane hydrate-bearing sediments with 40% porosity were carried out under the conditions of various hydrate dissociation times and temperatures. The following conclusions may be made:

1. The failure modes of methane hydrate-bearing sediments belonged to an elastic-plastic deformation and the stress–strain curves exhibited the shape of a hyperbola. The sediments exhibited a weak strain-softening type of behavior at the temperature of 5 °C.
2. Because the free methane gas produced by the hydrate dissociation entered into the pore space of sediments which resulted in a decrease in the effective confining pressure, the failure strength qf decreased with the increase of the methane hydrate dissociation time, and the rate of the decline of the failure strength qf was faster at the higher temperature.
3. Based on the experimental data and the nonlinear elastic Duncan-Chang model, the constitutive relation model of methane hydrate-bearing sediments as a function of temperature and dissociation time was proposed, and the developed model can be used effectively to predict most of the stress–strain curves, which exhibited a hardening type behavior in our experiment.

This study was focused on the homogeneous methane hydrate- bearing sediments. Actually, the homogeneity may affect the stability during hydrate dissociation and the examples of heterogeneous distribution should be investigated in further study

REFERENCES

Case I

[1]. E.D. Sloan Jr., C.A. Koh, Clathrate Hydrate of Natural Gases, 3rd Ed. Taylor & Francis-CRC Press, London, 2007.

[2]. E.D. Sloan Jr., Fundamental principles and applications of natural gas hydrates, Nature 426 (2003) 353–359.

[3]. J.S. Gudmundsson, M. Mork, O.F. Graff, Hydrate non-pipeline technology, 4th International Conference on Gas Hydrate, Yokohama, Japan, 2002, pp. 997–1002.

[4]. H. Kanda, Economic study on natural gas transportation with natural gas hydrate (NGH) pellets, 23rdWorld Gas Conference, Amsterdam, Netherlands, 2006, p. 11.

[5]. W. Hao, J. Wang, S. Fan, W. Hao, Evaluation and analysis method for natural gas hydrate storage and transportation process, Energy Conversion and Management 49 (2008) 2546–2553.

[6]. N.J. Kim, J.H. Lee, Y.S. Cho, W. Chun, Formation enhancement of methane hydrate for natural gas transport and storage, Energy 35 (2010) 2717–2722.

[7]. X. Lang, S. Fan, Y. Wang, Intensification of methane and hydrogen storage in clathrate hydrate and future prospect, Journal of Natural Gas Chemistry 19 (2010) 203–209.

[8]. B. Tohidi, A. Danesh, A.C. Todd, R.W. Burgass, K.K. Østergaard, Equilibrium data and thermodynamic modelling of cyclopentane and neopentane hydrates, Fluid Phase Equilibria 138 (1997) 241–250.

[9]. Y. Guo, S. Fan, K. Guo, Y. Chen, Storage capacity of methane in hydrate using calcium hypochlorite as additive, 4th International Conference on Gas Hydrate, Yokohama, Japan, 2002, pp. 1040–1043.

[10]. T. Uchida, R. Ohmura, I.Y. Ikada, J. Nagao, S. Takeya, A. Hori, Phase equilibrium measurements and crystallographic analyses on structure-H type gas hydrate formed from the CH4–CO2–neohexane–water system, The Journal of Physical Chemistry. B 110 (2006) 4583–4588.

[11]. B. Zhang, Q. Wu, D. Sun, Effect of surfactant tween on induction time of gas hydrate formation, Journal of China University of Mining and Technology 18 (2008) 0018–0021.

[12]. U. Karaaslan, E. Uluneye, M. Parlaktuna, Effect of an anionic surfactant on different type of hydrate structures, Journal of Petroleum Science and Engineering 35 (2002) 49–57.

[13]. H. Ganji, M. Manteghian, K. Sadaghiani zadeh, M.R. Omidkhah, H.R. Mofrad, Effect of different surfactants on methane hydrate formation rate, stability and storage capacity, Fuel 86 (2007) 434–441.

[14]. H. Ganji, M. Manteghian, H.R. Mofrad, Effect of mixed compounds on methane hydrate formation and dissociation rates and storage capacity, Fuel Processing Technology 88 (2007) 891–895.

[15]. Z. Sun, R. Wang, R. Ma, K. Guo, S. Fan, Natural gas storage in hydrates with the presence of promoters, Energy Conversion and Management 44 (2003) 2733–2742.

[16]. W. Wang, C.L. Bray, D.J. Adams, A.I. Cooper, Methane storage in dry water gas hydrates, Journal of the American Chemical Society 130 (2008) 11608–11609.

[17]. B.O. Carter, W. Wang, D.J. Adams, A.I. Cooper, Gas storage in “dry water” and “dry gel” clathrates, Langmuir 26 (2010) 3186–3193.

[18]. B.P. Binks, R. Murakami, Phase inversion of particle-stabilized materials from foams to dry water, Nature Materials 5 (2006) 865–869.

[19]. B.O. Carter, D.J. Adams, A.I. Cooper, Pausing a stir: heterogeneous catalysis in “dry water”, Green Chemsitry 12 (2010) 783–785.

[20]. Q. Chen, C. Liu, Y. Ye, Experimental study on geochemical characteristics of methane hydrate formed in porous media, Journal of Natural Gas Chemistry 18 (2009) 217–221.

Case II

[21]. Duncan, J.M., Chang, C.Y., 1970. Nonlinear analysis of stress and strain in soils. J. Soil Mech. Found.Div.96(5),1629–1653.

[22].Fu,S.Y.,Lu,J.A.,2010.Thecharacteristicsandoriginofgashydrateinshenhuarea, South ChinaSea.Mar.Geol.Lett.26(9),6–10.

[23].Hyodo,M.,Nakata,Y.,Yoshimoto,N.,Orense,R.,2007.Shearbehaviorofmethane hydrate-bearingsand. In:Proceedings of the 17th International Offshoreand Polar Engineering Conference. Lisbon, Portugal.

[24]. Hyodo, M.,Yoneda,J., Yoshimoto, N.,Nakata, Y., 2013. Mechanical and dissociation properties of methane hydrate-bearing sand in deep seabed. Soils Found.53 (2), 299–314.

[25]. Ji, C.,Ahmadi,G.,Smith,D.H.,2001.Natural gas production from hydrate decomposition by depressurization. Chem. Eng. Sci.56(20),5801–5814.

[26]. Kvenvolden,K.A.,1993.Gas hydrates-geological perspective and global change. Rev. Geophys. 31(2),173–187.

[27]. Kvenvolden,K.A.,1999.Potential effects of gas hydrate on human welfare. Proc. Natl. Acad. Sci. U.S. Am. 96(7),3420–3426.

[28]. Lee, J.Y., Santamarina, J.C.,Ruppel,C., 2010.Volume change associated with formation and dissociation of hydrate in sediment. Geochem. Geophys. Geosyst.11 (3).

[29]. Masui, A., Haneda, H., Ogata, Y., Aoki, K., 2007. Compaction behavior of Toyoura sand during methane hydrate dissociation. In: Seventh ISOPE Ocean Mining Symposium. Lisbon, Portugal.

[30]. Sloan, E.D., 2003. Fundamental principle sand applications of natural gas hydrates. Nature 426 (6964), 353–359